# Topological states in A15 superconductors

Minsung Kim,[1] Cai-Zhuang Wang,[1] and Kai-Ming Ho[1,2]
[1]*Ames Laboratory–U.S. Department of Energy, Iowa State University, Ames, Iowa 50011, USA*
[2]*Department of Physics and Astronomy, Iowa State University, Ames, Iowa 50011, USA*

(Received 25 July 2018; revised manuscript received 30 May 2019; published 12 June 2019)

Superconductors with the A15 structure are prototypical type-II *s*-wave superconductors which have generated considerable interest in early superconducting material history. However, the topological nature of the electronic structure remains unnoticed so far. Here, using first-principles band structure calculations based on density-functional theory, we show that the A15 superconductors ($Ta_3Sb$, $Ta_3Sn$, and $Ta_3Pb$) have nontrivial band topology in the bulk electronic band structures, leading to the formation of topological surface states near the Fermi energy. Due to the bulk superconductivity, the proximity effect in the topological surface states would induce topological superconductivity even without heterostructure of a topological insulator and an *s*-wave superconductor. Our results indicate that the A15 superconductors are promising candidates for the realization of the topological superconductivity and the Majorana fermion.

DOI: 10.1103/PhysRevB.99.224506

## I. INTRODUCTION

Topological phase of matter has been a central theme of recent condensed-matter physics [1,2]. An intriguing aspect of the topological states is that they are promising platforms to realize novel excitations such as Majorana fermions in condensed-matter systems, whereas they are elusive in high-energy physics [3–12]. One of the propositions to realize Majorana fermions is making heterostructures between strong topological insulators and *s*-wave superconductors, where the proximity-induced superconductivity in the topological surface states is analogous to that in a spinless $p_x + ip_y$ superconductor that is expected to have Majorana bound states at the vortices [4,5]. A straightforward extension of the idea would be to search for conventional *s*-wave superconductors which also have topological surface states [13–17]. The realization of topological superconductivity in a single material is advantageous considering the possible complexity at the interfaces of heterostructures.

A natural strategy for the search in this direction would be to examine existing superconductor material families in view of topological band theory. In conventional Bardeen-Cooper-Schrieffer (BCS) superconductors, the band structure in the normal phase is metallic and sizable density-of-states exist at the Fermi level. In contrast, the topological characterization of the band structure requires a band gap in order to define a topological invariant of the occupied band manifold since the band topology is defined using continuous deformation of the Hamiltonian without closing a gap. However, we note that it is still possible to define the band topology as long as there is a gap in the energy spectrum at each $k$ point (i.e., separate band manifolds). While the band structure of the superconductor would have metallic bands at the Fermi level, it is possible to have topological surface states in part of the Brillouin zone (BZ) where the metallic bulk bands do not overlap with them for appropriate surface termination. Thus, if we find a superconductor which has gaps at every $k$ point in the BZ with nontrivial band topology, it would be a potential candidate for the topological superconductor.

Here we show that superconductors with the A15 structure, which are representative metal-based superconductors mostly discovered between the 1950s and the 1970s [18–20], are promising candidates for topological superconductors. Specifically, $Ta_3Sb$, $Ta_3Sn$, and $Ta_3Pb$ are shown to have topological bulk band structures characterized by nontrivial $\mathbb{Z}_2$ invariants [21]. We find that the topological surface bands appear near the Fermi energy as dictated by the bulk-boundary correspondence [1]. Interestingly, since we have lower symmetry in the [001] surface, the topological surface states show nonhelical spin texture unlike, e.g., $Bi_2Se_3$ [22,23]. We also discuss the electronic band structures of Nb compounds in the A15 family.

Compared with recently discovered $FeSe_xTe_{1-x}$ [14–16], the A15 superconductor has the following differences and advantages. First, the spin configuration of the surface states in the A15 superconductor has more generalized form (see below for details). In the realization of the time-reversal symmetric proximity-induced surface topological superconductor, the minus sign required by Fermi statistics comes from $\pi$ Berry phase. Hence, in principle, any spin texture with $\pi$ Berry phase can be utilized. However, only helical spin configurations have been reported so far, including $FeSe_xTe_{1-x}$. Second, the energy window where surface states reside without overlap with bulk bands is relatively larger. In $FeSe_xTe_{1-x}$, the spin-orbit coupling (SOC) gap is reported to be about 10 meV, where the Dirac-cone-type surface states lie. In $Ta_3Sb$, for example, along $\bar{X}$–$\bar{\Gamma}$ of the surface BZ, direct bulk energy gap at each $k$ point is at least about 76 meV, which makes it easier to resolve the surface states using angle-resolved photoemission spectroscopy (ARPES). Third, the A15 superconductors are stoichiometric compounds which would have better material quality. Fourth, the pairing mechanism in the A15 superconductor is known to be conventional BCS

 

type, thus it is conceptually straightforward to understand the underlying physics.

## II. THEORETICAL METHODS

We performed first-principles electronic structure calculations based on density-functional theory as implemented in Vienna *ab initio* simulation package (VASP) [24,25]. We employed the projector augmented-wave method [26], and for the exchange correlation functional we adopted Perdew-Burke-Ernzerhof revised for solid (PBEsol) [27]. We used a plane-wave basis set with the energy cutoff of 325 eV, and $10 \times 10 \times 10$ $k$-point meshes were exploited. The experimental lattice constants were used [28–31] except for the case where we could not find an experimental value. For the surface-state calculations, we used 21-layer-thick slab models in the [001] direction with sufficiently large vacuum regions ($\gtrapprox$23 Å) to prevent the spurious interactions between the periodic images. The electronic structure was also checked and the symmetry property was analyzed using the Quantum espresso package [32].

## III. RESULTS AND DISCUSSIONS

The superconductors with the A15 structure have cubic symmetry with the space group $Pm\bar{3}n$ #223 [Fig. 1(c)]. They are intermetallic compounds with chemical formulas $A_3B$, where A atoms lie at the cube face of the unit cell forming mutually orthogonal one-dimensional chains along edges and B atoms constitute a bcc lattice. The crystal structure belongs to a nonsymmorphic space group where, for instance, we have a symmetry operation involving a screw axis,

$$\begin{pmatrix} x \\ y \\ z \end{pmatrix} \rightarrow \begin{pmatrix} \frac{1}{2} - y \\ \frac{1}{2} + x \\ \frac{1}{2} + z \end{pmatrix} = \begin{pmatrix} 0 & -1 & 0 \\ 1 & 0 & 0 \\ 0 & 0 & 1 \end{pmatrix} \begin{pmatrix} x \\ y - \frac{1}{2} \\ z \end{pmatrix} + \begin{pmatrix} 0 \\ \frac{1}{2} \\ \frac{1}{2} \end{pmatrix}, \quad (1)$$

with the lattice constant set to 1 for simplicity. This operation is a fourfold rotation around the $z$ axis with respect to $(0, 1/2, 0)$ followed by a fractional translation along the $z$ direction. Accordingly, we have fourfold rotational symmetry in the bulk electronic band structure although we do not have the strict fourfold rotation in the crystal structure.

The electronic band structure of the representative superconductor $Ta_3Sb$ shows metallic feature with separate band manifolds, i.e., separation of the "valence" and the "conduction" bands in the whole BZ as shown in Fig. 1(a). We find that SOC is essential to have the separation of the band manifolds [Figs. 1(a) and 1(b)]. The bands near the Fermi energy mostly have Ta $d$ character. Since the crystal structure possesses the spatial inversion symmetry, the band topology of the valence bands can be calculated from the parities of the wave functions at the time-reversal invariant momenta (TRIM) [33]. The parity products are $+$, $+$, $-$, and $+$ for $\Gamma$, $3X$, $3M$, and $R$, respectively, which results in a strong topological phase with $(\nu_0; \nu_1\nu_2\nu_3) = (1; 000)$, where $\nu_0$ is the strong $\mathbb{Z}_2$ index and $\nu_1$, $\nu_2$, $\nu_3$ are the weak ones [Fig. 1(d)]. Here the strong index is determined from the product of the parities at all eight TRIM, and the weak indices from the product at four TRIM

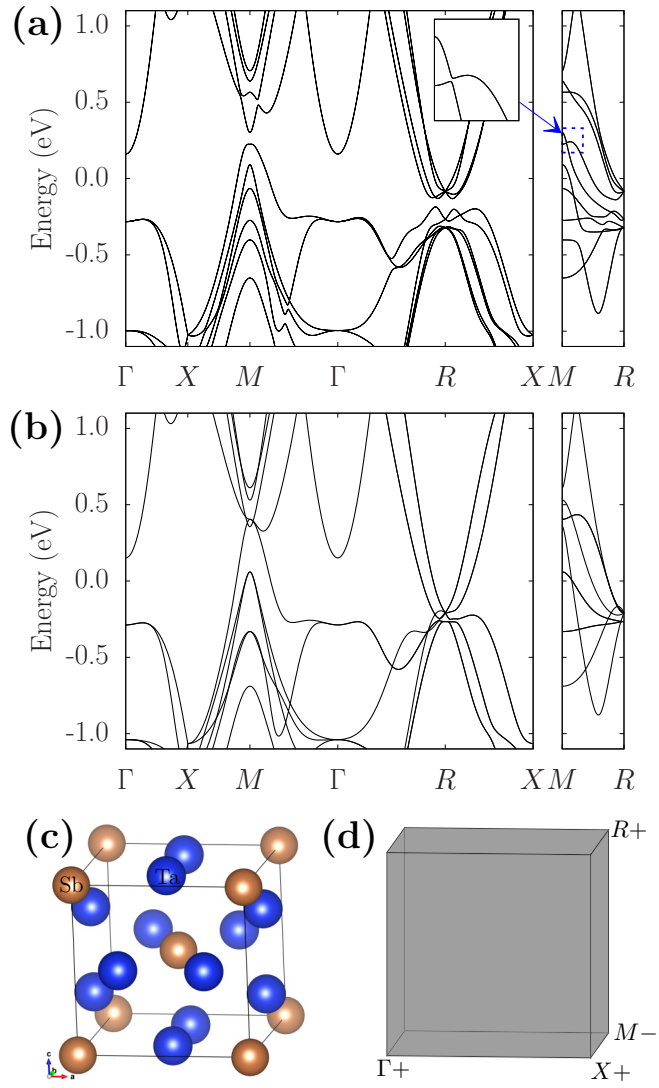


FIG. 1. Electronic band structure and atomic structure of $Ta_3Sb$. The band structure along high-symmetry paths in the BZ (a) with and (b) without SOC. (c) The atomic structure of $Ta_3Sb$. (d) The parity products in the BZ. The Fermi energy is set to 0.

in $k_i = \pi$ $(i = x, y, z)$ planes with the lattice constant set to 1. We also check the electronic band structure with modified Becke-Johnson (MBJ) potential which gives more accurate results for the band energy and the band gap [34,35] (see the Appendix for the MBJ band structure). We confirm that the band structure does not change qualitatively, and the band topology remains the same.

One of the direct consequences of the nontrivial bulk band topology is the existence of the topological surface bands. In the [001] surface of $Ta_3Sb$, we indeed find topological surface states as shown in Fig. 2(a). The number (mod 2) of crossings between the surface states and a line connecting two TRIM of the surface BZ in the gaps is dictated by the projected parity products. For example, since we have different parities at $\bar{\Gamma}$ and $\bar{X}$ (i.e., $+$ at $\bar{\Gamma}$ and $-$ at $\bar{X}$), an odd number of crossings occurs along $\bar{\Gamma}$–$\bar{X}$ [Fig. 2(a)], which characterizes

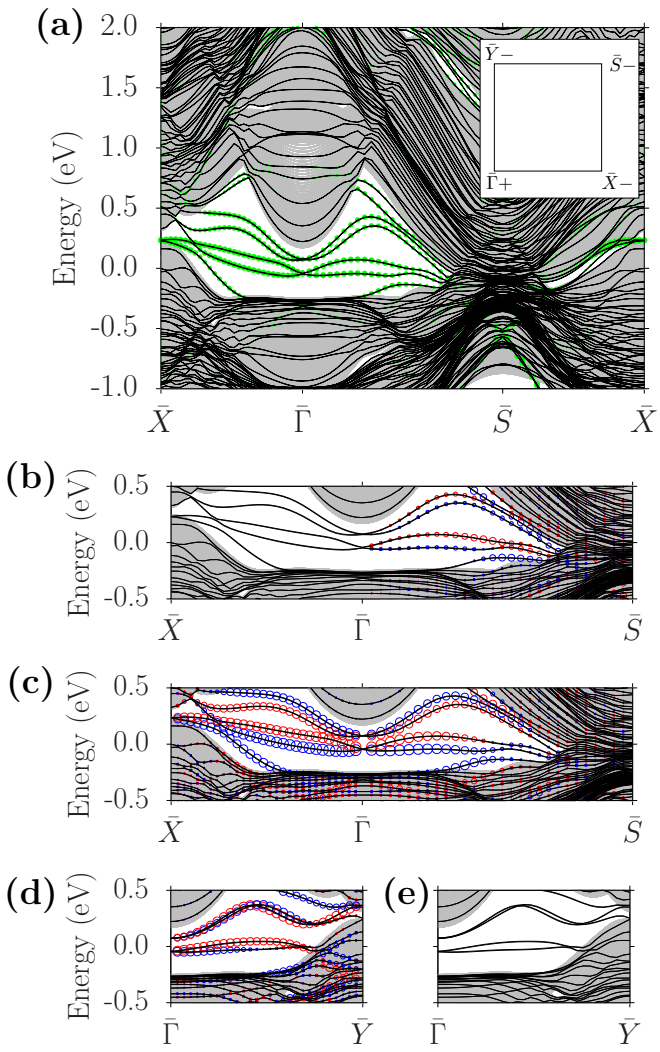


FIG. 2. Surface states of $Ta_3Sb$ in the [001] surface. (a) Electronic band structure along high-symmetry paths in the surface BZ. Green circles denote the surface contribution. The inset shows the projected parity products at TRIM. [(b) and (d)] The $x$ component of the spin angular momentum. [(c) and (e)] The $y$ component of the spin angular momentum. The red and blue circles denote the positive and negative values, respectively. The gray regions correspond to the projected bulk states.

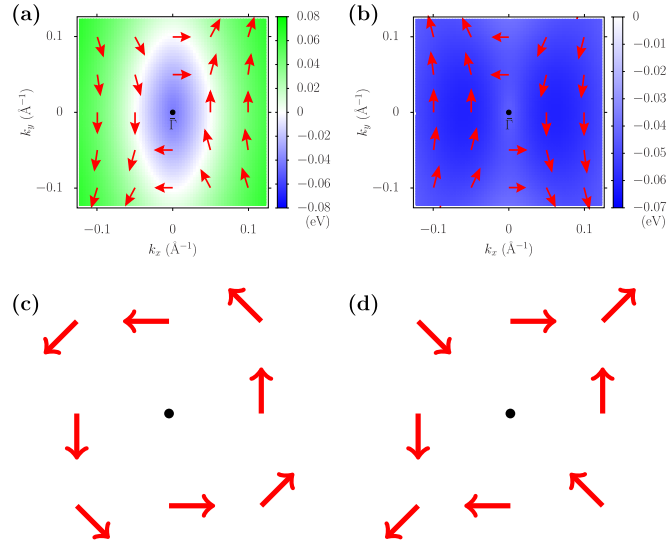


FIG. 3. Spin angular-momentum texture of surface states near $\bar{\Gamma}$ in the [001] surface of $Ta_3Sb$. The spin texture of the (a) lower and (b) upper bands. Green and blue colors represent the band energy with respect to the Fermi level as indicated in the color bar. The schematic illustration of (c) helical (Rashba-type) spin texture and (d) linear Dresselhaus-type one.

topological surface states. This confirms the bulk-boundary correspondence between the bulk topological invariants and the surface-state configurations.

The spin-polarized surface states have nonhelical spin structure (as opposed to typical helical surface states, e.g., in $Bi_2Se_3$) due to the reduced symmetry at the [001] surface (Fig. 2). In general, topological surface states are spin-polarized due to the SOC and the breaking of the inversion symmetry at the surface. The specific spin configuration is determined by the relevant symmetry of the terminated surface, whereas we have the fourfold symmetry in the bulk electronic bands, we have only twofold symmetry in the [001] surface since the symmetry involving the fractional translation is broken. The symmetry reduction at the surface is important for the qualitative understanding of the spin configuration. To see this, we consider the effective Hamiltonian $H_{\text{eff}} = \mathcal{A}k_y\sigma_x - \mathcal{B}k_x\sigma_y$ which is the general form under $C_{2v}$ (the relevant symmetry of the surface states near $\bar{\Gamma}$) and the time-reversal symmetry up to linear order in $k$. Here $\sigma$'s are Pauli matrices that describe the spin degree of freedom. $H_{\text{eff}}$ gives an anisotropic Dirac cone with the energy eigenvalues $E = \pm|\mathbf{k}|\sqrt{\mathcal{A}^2\sin^2\theta_{\mathbf{k}} + \mathcal{B}^2\cos^2\theta_{\mathbf{k}}}$, in which $\cos\theta_{\mathbf{k}} = k_x/|\mathbf{k}|$ and $\sin\theta_{\mathbf{k}} = k_y/|\mathbf{k}|$. When the local $k$ axis is rotated by $\pi/4$, the Hamiltonian takes the form $\alpha_R(k_y\sigma_x - k_x\sigma_y) + \alpha_D(k_x\sigma_x - k_y\sigma_y)$ with $\alpha_R = (\mathcal{A}+\mathcal{B})/2$ and $\alpha_D = (\mathcal{A}-\mathcal{B})/2$. Here the $\alpha_R$ term gives rise to helical (Rashba-type) spin texture [Fig. 3(c)], and the $\alpha_D$ term leads to linear Dresselhaus-type one [Fig. 3(d)] [36,37]. Indeed, our first-principles calculations show that the resulting spin configuration of the surface states near the Fermi energy around $\bar{\Gamma}$ is a mixture of the two types of spin textures [Fig. 3(a)]. Note that under higher symmetry $C_{4v}$ or $C_{3v}$ we should have $\mathcal{A} = \mathcal{B}$, i.e., only the $\alpha_R$ (helical) term survives. If the screw rotation is changed to conventional rotation, then the [001] surface would have $C_{4v}$ symmetry, allowing only helical spin configuration.

Now we discuss the proximity-induced superconductivity in the surface states. Here we consider the simplest case under the $C_{2v}$ symmetry and the time-reversal symmetry, where we have a single Dirac cone at the $\bar{\Gamma}$ point. If we substitute $k'_x = \frac{\mathcal{B}}{v}k_x$ and $k'_y = \frac{\mathcal{A}}{v}k_y$ with $v = \sqrt{\mathcal{A}^2+\mathcal{B}^2}$ in the effective Hamiltonian, the Hamiltonian becomes mathematically analogous to the isotropic helical Dirac cone described by $v(k'_y\sigma_x - k'_x\sigma_y)$. The analysis can be given in a similar way with Ref. [5] except for the spin helicity. We consider the Cooper pairs tunneling into the surface states due to the proximity effect by introducing $H_{\text{p}} = \Delta\psi^\dagger_\uparrow\psi^\dagger_\downarrow + \text{H.c.}$ with $\Delta = \Delta_0 e^{i\phi}$. Then the Bogoliubov–de Gennes (BdG) Hamiltonian is given by

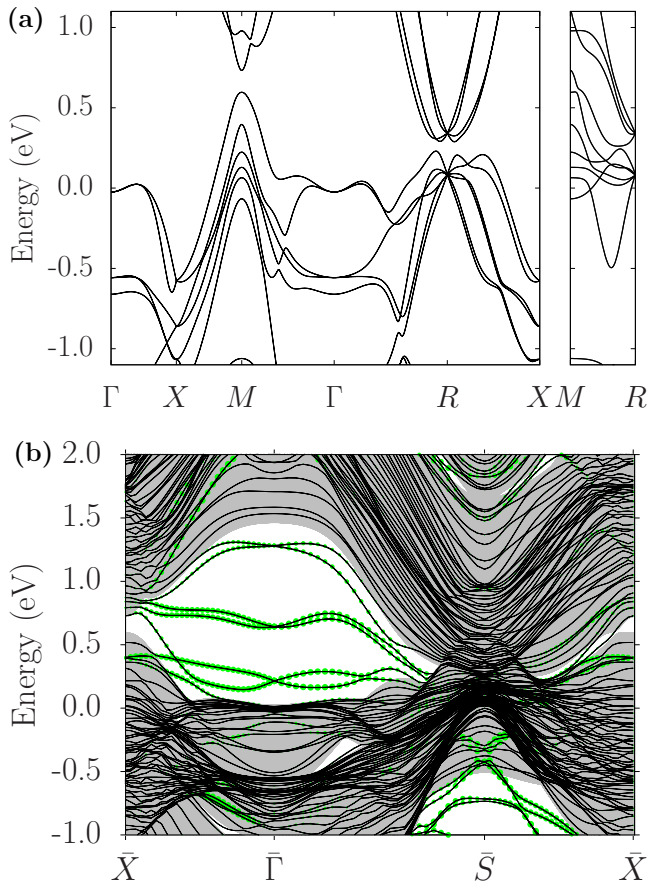


FIG. 4. Electronic structure of $Ta_3Sn$. (a) Bulk band structure along high-symmetry paths in $Ta_3Sn$. (b) Band structure of the [001] surface. Green circles denote the surface contribution. The Fermi level is set to 0.

$H_{\mathrm{BdG}} = \frac{1}{2}\Psi^{\dagger}\mathcal{H}_{\mathrm{BdG}}\Psi$, where

$$\mathcal{H}_{\mathrm{BdG}} = \begin{bmatrix} -iv(\sigma_x\partial_y - \sigma_y\partial_x) - \mu & \Delta \\ \Delta^* & iv(\sigma_x\partial_y - \sigma_y\partial_x) + \mu \end{bmatrix}, \quad (2)$$

and $\Psi = (\psi_\uparrow, \psi_\downarrow, \psi_\downarrow^\dagger, -\psi_\uparrow^\dagger)^T$ with $\mu$ being the chemical potential. By solving the BdG equation $\mathcal{H}_{\mathrm{BdG}}\zeta = E\zeta$ for a vortexlike condition $\Delta = \Delta_0(r)e^{i\theta}$ in polar coordinates, the zero energy bound states can be found. The solution for $\mu = 0$ case is simple and can be written as

$$\zeta(r,\theta) = \begin{pmatrix} 1 \\ 0 \\ 0 \\ -1 \end{pmatrix} \exp\left[ -\int_0^r ds \frac{\Delta_0(s)}{v} \right], \quad (3)$$

which represents the Majorana zero mode localized at the vortex.

Although our model assumed the simple surface band structure with a single anisotropic Dirac cone, the surface band structure from our DFT calculation is more complicated having accidental surface bands as well as topological ones. The accidental surface states can be removed from the Fermi energy by changing the surface potential, whereas the topological ones are guaranteed to remain gapless by the nontrivial bulk topological order. In principle, if we change the surface potential properly, then it could be possible to have simpler surface band structure having only a single time-reversal pair of surface bands at the Fermi level.

The electronic band structure of $Ta_3Sn$ shows qualitatively the same band topology. Since we substitute Sb (Group VA in the periodic table) with Sn (Group IVA), the Fermi energy moves downward below the surface states (Fig. 4). The experimental superconducting transition temperatures ($T_c$) of $Ta_3Sb$ and $Ta_3Sn$ are 0.7 K and 8.3 K, respectively [18]. We also find nontrivial band topology in $Ta_3Pb$ (Pb also belongs to Group IVA) which has $T_c = 17$ K [19]. The compounds with Sn or Pb have the advantage that they have higher $T_c$ while electron doping would be needed to adjust the Fermi level in the surface. The manipulation of the Fermi level in the surface layers could be possible using chemical substitution or liquid gating [38,39].

Another variation of the composition would be the substitution of Ta with Nb since they belong to the same group in the periodic table. However, we find that the valence and the conduction bands in $Nb_3Sb$ and $Nb_3Sn$ are not separated unlike the Ta compounds probably due to the weaker SOC strength of Nb. Thus, the $\mathbb{Z}_2$ bulk band topology is not properly defined in the Nb compounds.

## IV. CONCLUSION

In conclusion, we reported hitherto-unnoticed topological phases in A15 superconductors, $Ta_3Sb$, $Ta_3Sn$, and $Ta_3Pb$. The topological band structure was characterized by the nontrivial strong $\mathbb{Z}_2$ topological invariant $\nu_0 = 1$. Corresponding topological surface states appear in the [001] surface, and they show nonhelical spin texture due to the reduced symmetry at the surface. The proximity-induced superconductivity at the surface would give rise to the Majorana zero mode. The topological surface bands of the proposed compounds could be experimentally verified using ARPES [1,40]. Our study shows that the A15 superconductors are promising candidates for the realization of the topological superconductivity and Majorana fermions and potentially useful for topological quantum computation.

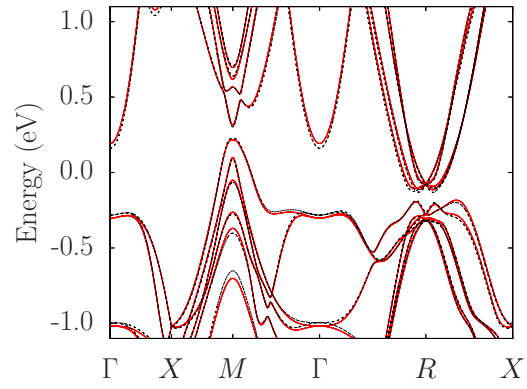


FIG. 5. Electronic band structure of $Ta_3Sb$ using MBJ potential. The red solid and black dotted lines show the band structures with the MBJ and PBEsol, respectively.

## ACKNOWLEDGMENTS

We thank Suk Bum Chung for fruitful discussions. This work was supported by the US Department of Energy (DOE), Office of Science, Basic Energy Sciences, Materials Sciences and Engineering Division. The research was performed at Ames Laboratory, which is operated for the US DOE by Iowa State University under Contract No. DE-AC02-07CH11358. Computations were performed through the support of the National Energy Research Scientific Computing Center, which is a DOE Office of Science User Facility operated under Contract No. DE-AC02-05CH11231.


## APPENDIX: ELECTRONIC BAND STRUCTURE WITH THE MBJ POTENTIAL

The electronic band structure of $Ta_3Sb$ using MBJ potential is presented in Fig. 5.


[1] M. Z. Hasan and C. L. Kane, Rev. Mod. Phys. **82**, 3045 (2010).
[2] X.-L. Qi and S.-C. Zhang, Rev. Mod. Phys. **83**, 1057 (2011).
[3] E. Majorana, Nuovo Cimento **14**, 171 (1937).
[4] N. Read and D. Green, Phys. Rev. B **61**, 10267 (2000).
[5] L. Fu and C. L. Kane, Phys. Rev. Lett. **100**, 096407 (2008).
[6] G. E. Volovik, JETP Lett. **90**, 398 (2009).
[7] J. D. Sau, R. M. Lutchyn, S. Tewari, and S. Das Sarma, Phys. Rev. Lett. **104**, 040502 (2010).
[8] J. Alicea, Phys. Rev. B **81**, 125318 (2010).
[9] J. Linder, Y. Tanaka, T. Yokoyama, A. Sudbø, and N. Nagaosa, Phys. Rev. Lett. **104**, 067001 (2010).
[10] M. Wimmer, A. R. Akhmerov, M. V. Medvedyeva, J. Tworzydło, and C. W. J. Beenakker, Phys. Rev. Lett. **105**, 046803 (2010).
[11] R. M. Lutchyn, J. D. Sau, and S. Das Sarma, Phys. Rev. Lett. **105**, 077001 (2010).
[12] Y. Oreg, G. Refael, and F. von Oppen, Phys. Rev. Lett. **105**, 177002 (2010).
[13] B. Yan, M. Jansen, and C. Felser, Nat. Phys. **9**, 709 (2013).
[14] P. Zhang, K. Yaji, T. Hashimoto, Y. Ota, T. Kondo, K. Okazaki, Z. Wang, J. Wen, G. D. Gu, H. Ding, and S. Shin, Science **360**, 182 (2018).
[15] Z. Wang, P. Zhang, G. Xu, L. K. Zeng, H. Miao, X. Xu, T. Qian, H. Weng, P. Richard, A. V. Fedorov, H. Ding, X. Dai, and Z. Fang, Phys. Rev. B **92**, 115119 (2015).
[16] G. Xu, B. Lian, P. Tang, X.-L. Qi, and S.-C. Zhang, Phys. Rev. Lett. **117**, 047001 (2016).
[17] S.-Y. Guan, P.-J. Chen, M.-W. Chu, R. Sankar, F. Chou, H.-T. Jeng, C.-S. Chang, and T.-M. Chuang, Sci. Adv. **2**, e1600894 (2016).
[18] A. Narlikar, *Superconductors* (Oxford University Press, Oxford, 2014).
[19] K. Buschow, *Concise Encyclopedia of Magnetic and Superconducting Materials*, Advances in Materials Sciences and Engineering (Elsevier Science, Amsterdam, 2005).
[20] H. Hosono, A. Yamamoto, H. Hiramatsu, and Y. Ma, Mater. Today **21**, 278 (2018).
[21] L. Fu, C. L. Kane, and E. J. Mele, Phys. Rev. Lett. **98**, 106803 (2007).
[22] H. Zhang, C.-X. Liu, X.-L. Qi, X. Dai, Z. Fang, and S.-C. Zhang, Nat. Phys. **5**, 438 (2009).
[23] W. Zhang, R. Yu, H.-J. Zhang, X. Dai, and Z. Fang, New J. Phys. **12**, 065013 (2010).
[24] G. Kresse and J. Hafner, Phys. Rev. B **47**, 558 (1993).
[25] G. Kresse and J. Furthmüller, Phys. Rev. B **54**, 11169 (1996).
[26] P. E. Blöchl, Phys. Rev. B **50**, 17953 (1994).
[27] J. P. Perdew, A. Ruzsinszky, G. I. Csonka, O. A. Vydrov, G. E. Scuseria, L. A. Constantin, X. Zhou, and K. Burke, Phys. Rev. Lett. **100**, 136406 (2008).
[28] H. L. Luo, E. Vielhaber, and E. Corenzwit, Z. Physik **230**, 443 (1970).
[29] T. H. Courtney, G. W. Pearsall, and J. Wulff, J. Appl. Phys. **36**, 3256 (1965).
[30] S. Furuseth and A. Kjekshus, Acta Chem. Scand. **18**, 1180 (1964).
[31] I. Guseva, Y. Seropegin, and E. Sokolovskaya, J. Less Common Metals **87**, 109 (1982).
[32] P. Giannozzi, S. Baroni, N. Bonini, M. Calandra, R. Car, C. Cavazzoni, D. Ceresoli, G. L. Chiarotti, M. Cococcioni, I. Dabo, A. D. Corso, S. de Gironcoli, S. Fabris, G. Fratesi, R. Gebauer, U. Gerstmann, C. Gougoussis, A. Kokalj, M. Lazzeri, L. Martin-Samos, N. Marzari, F. Mauri, R. Mazzarello, S. Paolini, A. Pasquarello, L. Paulatto, C. Sbraccia, S. Scandolo, G. Sclauzero, A. P. Seitsonen, A. Smogunov, P. Umari, and R. M. Wentzcovitch, J. Phys.: Condens. Matter **21**, 395502 (2009).
[33] L. Fu and C. L. Kane, Phys. Rev. B **76**, 045302 (2007).
[34] A. D. Becke and E. R. Johnson, J. Chem. Phys. **124**, 221101 (2006).
[35] F. Tran and P. Blaha, Phys. Rev. Lett. **102**, 226401 (2009).
[36] M. Kim, J. Ihm, and S. B. Chung, Phys. Rev. B **94**, 115431 (2016).
[37] A. Stroppa, D. Di Sante, P. Barone, M. Bokdam, G. Kresse, C. Franchini, M.-H. Whangbo, and S. Picozzi, Nat. Commun. **5**, 5900 (2014).
[38] J. T. Ye, S. Inoue, K. Kobayashi, Y. Kasahara, H. T. Yuan, H. Shimotani, and Y. Iwasa, Nat. Mater. **9**, 125 (2010).
[39] J. Jeong, N. Aetukuri, T. Graf, T. D. Schladt, M. G. Samant, and S. S. P. Parkin, Science **339**, 1402 (2013).
[40] D. Hsieh, D. Qian, L. Wray, Y. Xia, Y. S. Hor, R. J. Cava, and M. Z. Hasan, Nature **452**, 970 (2008).